

# Interpretable Single-Cell Set Classification with Kernel Mean Embeddings

Siyuan Shan<sup>1</sup>, Vishal Baskaran<sup>1</sup>, Haidong Yi<sup>1</sup>, Jolene Ranek<sup>2,3</sup>, Natalie Stanley<sup>1,2</sup>, Junier Oliva<sup>1</sup>

<sup>1</sup> Department of Computer Science, University of North Carolina at Chapel Hill

<sup>2</sup> Computational Medicine Program, The University of North Carolina at Chapel Hill

<sup>3</sup> Curriculum in Bioinformatics and Computational Biology, The University of North Carolina at Chapel Hill

**Abstract.** Modern single-cell flow and mass cytometry technologies measure the expression of several proteins of the individual cells within a blood or tissue sample. Each profiled biological sample is thus represented by a set of hundreds of thousands of multidimensional cell feature vectors, which incurs a high computational cost to predict each biological sample’s associated phenotype with machine learning models. Such a large set cardinality also limits the interpretability of machine learning models due to the difficulty in tracking how each individual cell influences the ultimate prediction. Using Kernel Mean Embedding to encode the cellular landscape of each profiled biological sample, we can train a simple linear classifier and achieve state-of-the-art classification accuracy on 3 flow and mass cytometry datasets. Our model contains few parameters but still performs similarly to deep learning models with millions of parameters. In contrast with deep learning approaches, the linearity and sub-selection step of our model make it easy to interpret classification results. Clustering analysis further shows that our method admits rich biological interpretability for linking cellular heterogeneity to clinical phenotype. Our codes are publicly available at <https://github.com/shansiliu95/CKME>.

**Keywords:** Cytometry · Single-Cell Bioinformatics · Clinical Prediction · Flow Cytometry · Mass Cytometry · Kernel Methods

## 1 Introduction

Modern immune profiling techniques, such as, flow and mass cytometry (CyTOF) enable comprehensive profiling of immunological heterogeneity across a multi-patient cohort [10,16]. In recent years, such technologies have been applied for numerous clinical applications. In particular, these assays allow for both the phenotypic and functional characterization of immune cells based on the simultaneous measurement of 10-45 protein markers [3]. To further connect the diversity, abundance, and functional state of specific immune cell-types to clinical outcomes or external variables, modern bioinformatics approaches have focused on how to engineer or learn a set of “immune features” that adequately encodes a profiled individual’s immunological landscape. In general, existing approaches for creating immunological features either rely heavily on manual human effort [14,12,16], clustering [5,21,25], or do not

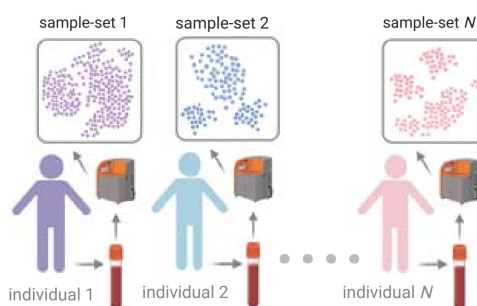


Fig. 1: Single-cell profiles produce a *sample-set* of (typically thousands of) multidimensional feature vectors of measured features per cell (illustrated as scatter plots). Thus, a dataset of multiple biological samples will result in a dataset of multiple sets (shown above).

produce immunological features that are readily interpretable or informative for follow-up experiments, diagnostics, or treatment strategies [27,15,2]. To efficiently and accurately link cellular heterogeneity to clinical outcomes or external variables, here we introduce CKME (Cell Kernel Mean Embedding), a method based on kernel mean embeddings [19]. We show that CKME is simple enough to be readily interpreted by a human, and achieves state-of-the-art classification accuracy in clinical outcome prediction tasks.

**Flow and Mass Cytometry Assays Produce a Dataset of Sets** To comprehensively profile the immune systems of biological samples collected across multiple individuals, a unique data structure of multiple *sample-sets* is ultimately produced. Each sample-set is likely to contain hundreds of thousands of cells collected from an individual, and machine learning models are often used to predict their associated clinical or experimental labels. This concept is illustrated in Fig. 1. In profiling multiple individuals with a single-cell technology, a *dataset of sets* is produced and is a non-traditional data structure that breaks the standard convention of a *dataset of feature vectors*. This produces complexity for learning over individuals (e.g. patients), as single-cell data requires a model to characterize and compare across multiple sets of multiple vectors (where each vector represents a cell). Another challenge of analyzing single-cell data is the large number of cells in each sample-set, which incurs a computational cost and obscures the decision-making process of machine learning models.

**Related Work** The first class of methods for identifying coherent cell-populations and specifying their associated immunological features are *gating-based*<sup>1</sup>, and operate by first assigning cells to populations either manually, or in an automated manner by applying an unsupervised clustering approach [16]. After an individual’s cells have been assigned to their respective cell-populations, corresponding immunological features are specified by 1) computing frequencies or the proportion of cells assigned to each population and 2) computing functional readouts as the median expression of a particular functional marker [25]. These approaches are effective in practice and are readily interpretable for communication, but tend to be sensitive to variation in the parameters of the underlying clustering algorithms.

The second class of methods are *gating-free* and rely on representing, or making predictions based on individual cells [2,15,27]. For example, CytoDX [15] uses a linear model to predict the class label of each cell’s corresponding sample set. Ultimately, the predicted label of a sample-set is the mean of the predicted labels across all cells. Alternatively, CellCNN [2] and CytoSet [27] leverage deep learning approaches to learn a representation for each individual cell and ultimately pool these representations to encode the entire sample-set. These strategies achieve strong prediction quality but lack interpretability, as deep learning models usually contain millions of parameters and a single prediction can require millions of mathematical operations that are difficult for humans to understand [18].

**Summary and Contribution of Results** In this work, we tackle the challenges highlighted above by computing a kernel mean embedding of sample-sets [19], to represent sample-sets using averages across features of respective elements. For classification tasks, we train a linear classifier (e.g. logistic regression or linear SVM) in the feature space. Despite the simplicity, CKME achieves state-of-the-art accuracies on three flow and mass cytometry datasets with multiple sample-sets and associated clinical outcomes. We also discover that CKME readily enables the biological interpretation of the prominent cells driving a classification result as an average of individual cell responses. As a result, CKME is highly interpretable since one can quantify the individual contribution of every cell to the final prediction. Predictions are then synthesized further using kernel herding [8], which identifies key cells to retain in a subsample. Lastly, the individual cell responses computed by CKME can also be seamlessly combined with unsupervised clustering analysis

<sup>1</sup> Gating refers to partitioning cells into populations

to provide further interpretation.

## 2 Methods

**Notation for Sample-sets** A *sample-set* refers to the collection of cells from an individual’s blood or tissue, and is further represented as a sample-set of many,  $n$ , cells:  $\mathcal{X} = \{x^{(i)}\}_{i=1}^n$ , where  $x^{(i)} \in \mathbb{R}^d$  denotes the vector of  $d$  features (e.g. proteins or genes) measured in cell  $i$ . A multi-sample dataset  $\mathcal{D}$  contains multiple sample-sets (across multiple,  $N$ , individuals and conditions):  $\mathcal{D} = \{\mathcal{X}^{(k)}\}_{k=1}^N = \{\{x^{(k,i)}\}_{i=1}^{n_k}\}_{k=1}^N$ , where  $\mathcal{X}^{(k)} = \{x^{(k,i)}\}_{i=1}^{n_k}$  is the sample-set for the  $k$ -th profiled biological sample. Sample-sets often have an associated labels of interest,  $y$ , such as their clinical phenotype or conditions. In this case, our dataset consists of sample-set and label tuples:  $\mathcal{D} = \{(\mathcal{X}^{(k)}, y^{(k)})\}_{k=1}^N$ .

**Problem Formulation** Given a dataset of multiple sample-sets as discussed above, we wish to build a discriminative model  $p(y|\mathcal{X})$  to predict patient-level phenotypes or conditions based on the cellular composition that is found within a sample-set. If the model is human interpretable, it will help to make sense of how the cell feature vectors in a sample-set influence the predicted phenotype or conditions of a patient, which eventually will lead to an improved understanding of biological phenomena and enable better diagnoses and treatment for patients. Below we propose a methodology to featurize and classify input sample-sets in a way that is more transparent and human-understandable than comparably performant models (e.g. [27]).

**Kernel Mean Embedding** To classify labels of interest,  $y$ , given an input sample-set,  $\mathcal{X}$ , we featurize  $\mathcal{X}$  so that we may learn an estimator over those features. However, unlike traditional data-analysis, which featurizes a single vector instance  $x \in \mathbb{R}^d$  with features  $\phi(x) : \mathbb{R}^d \mapsto \mathbb{R}^q$ , here we featurize a *set of multiple* vectors (one vector for each cell in a sample-set)  $\mathcal{X} = \{x^{(i)}\}_{i=1}^n$ ,  $\phi(\mathcal{X}) \in \mathbb{R}^q$ .

Featurizing a set presents a myriad of challenges since typical machine learning approaches are constructed for *statically-sized, ordered* inputs. In contrast, sets are of *varying cardinalities* and are *unordered*. Hence, straight-forward approaches, such as concatenating the sample-set elements into a single vector  $(x^{(1)}, \dots, x^{(n)}) \in \mathbb{R}^{nd}$  shall fail to provide mappings that do not depend on the order that elements appear in. To respect the *unordered* property of sample-sets one must carefully featurize  $\mathcal{X}$  in a way that is *permutation-invariant*. That is, the features  $\phi(\mathcal{X})$  should be unchanged regardless of what order that the elements of  $\mathcal{X}$  are processed. Recently, there have been multiple efforts to create methods based on neural networks to featurize sets in a permutation invariant manner [20,28,24]. Although these approaches provide expressive, non-linear, discriminative features, they are often opaque and difficult to understand in how they lead to their ultimate predictions. In contrast, we propose an approach based on kernels and random features that is more transparent and understandable whilst being comparably accurate.

Kernel methods have achieved great success in many distinct machine learning tasks, including: classification [9], regression [26], and dimensionality reduction [17]. They utilize a positive definitive kernel function  $\mathbf{k} : \mathbb{R}^d \times \mathbb{R}^d \mapsto \mathbb{R}^2$ , which induces a reproducing kernel Hilbert space (RKHS) (e.g. see [4] for further details). Kernels have also been deployed for representing a distribution,  $p$ , with the *kernel mean embedding*  $\mu_p : \mathbb{R}^d \mapsto \mathbb{R}$ :

$$\mu_p(\cdot) \equiv \mathbb{E}_{x \sim p}[\mathbf{k}(x, \cdot)]. \quad (1)$$

Note that  $\mu_p$  is itself a function. For “*characteristic*” kernels,  $\mathbf{k}$ , such as the common radial-basis function (RBF) kernel  $\mathbf{k}(x, x') = \exp(-\frac{1}{2\gamma}\|x - x'\|^2)$ , the kernel mean embedding will be unique to its distribution;

<sup>2</sup> Note that kernels may be defined over non-real domains, this is omitted for simplicity.

i.e., for characteristic kernels,  $\|\mu_p - \mu_q\| = 0$  if and only if  $p = q$ . In general, the distance<sup>3</sup>  $\|\mu_p - \mu_q\|$  induces a divergence, the maximum mean discrepancy (MMD) [13], between distributions.

For our purposes, we propose to use kernel mean embeddings to featurize sample-sets:

$$\mu_{\mathcal{X}}(\cdot) \equiv \frac{1}{n} \sum_{i=1}^n \mathbf{k}(x^{(i)}, \cdot) \approx \mu_p(\cdot), \quad (2)$$

where  $p$  is the underlying distribution (of cell features) that  $\mathcal{X}$  was sampled from. That is, the set embedding  $\mu_{\mathcal{X}}$  (eq. 2) also approximately embeds the underlying distribution of cells that the sample-set was derived from. To produce a real-valued output from the mean embedding, one would take the (RKHS) inner product with a learned function  $f$ :

$$\langle \mu_{\mathcal{X}}, f \rangle = \frac{1}{n} \sum_{i=1}^n \langle \mathbf{k}(x^{(i)}, \cdot), f(\cdot) \rangle = \frac{1}{n} \sum_{i=1}^n f(x^{(i)}), \quad (3)$$

where the last term follows from the reproducing property of the RKHS. For example, eq. 3 can be used to output the log-odds for a target  $y$  given  $\mathcal{X}$ :  $p(y = 1|\mathcal{X}) = (1 + \exp(-\langle \mu_{\mathcal{X}}, f \rangle))^{-1}$ . Using the representer theorem [23] it can be shown that  $f$  may be learned and represented using a “Gram” matrix of pairwise kernel evaluations,  $\mathbf{k}(x, x')$ . This, however, will be prohibitive in larger datasets. Instead of working directly with a kernel  $\mathbf{k}$ , we propose to leverage random Fourier features for computational efficiency and simplicity.

**Random Fourier Features** We propose to use random Fourier frequency features [22] to build our mean embedding [19]. For a shift-invariant kernel (such as the RBF kernel), random Fourier features provide a feature map  $\varphi(x) \in \mathbb{R}^D$  such that the dot product in feature space approximates the kernel evaluation,  $\varphi(x)^T \varphi(x') \approx \mathbf{k}(x, x')$ . I.e.  $\varphi(x)$  acts as an approximate *primal space* for the kernel  $\mathbf{k}$ . Using the dot product of  $\varphi(x)$ , our mean embedding becomes

$$\mu_{\mathcal{X}} = \frac{1}{n} \sum_{i=1}^n \varphi(x^{(i)}) \in \mathbb{R}^D, \quad \mu_{\mathcal{X}}(x') = \frac{1}{n} \sum_{i=1}^n \varphi(x^{(i)})^T \varphi(x') \quad (4)$$

where  $\varphi(x) = (\sin(\omega_1^T x), \dots, \sin(\omega_{D/2}^T x), \cos(\omega_1^T x), \dots, \cos(\omega_{D/2}^T x))$  with random frequencies  $\omega_j \sim \rho$  drawn once (and subsequently held fixed) from a distribution  $\rho$  that depends on the kernel  $\mathbf{k}$ . For instance, for the RBF kernel  $\rho$  is an iid multivariate independent normal with mean 0 and variance that depends on the bandwidth of the kernel,  $\gamma$ . When computing the mean embedding in the  $\varphi(\cdot)$  feature space (eq. 4), one may directly map  $\mu_{\mathcal{X}}$  to a real value with a dot product with learned coefficient  $\beta \in \mathbb{R}^D$ :

$$\mu_{\mathcal{X}}^T \beta = \left( \frac{1}{n} \sum_{i=1}^n \varphi(x^{(i)}) \right)^T \beta = \frac{1}{n} \sum_{i=1}^n \varphi(x^{(i)})^T \beta. \quad (5)$$

That is, we may learn a linear model directly operating over the  $D$  dimensional feature vectors  $\mu_{\mathcal{X}}$ , which are composed of the average random features found in a sample-set. Below we expound on how to build a discriminative model based on  $\mu_{\mathcal{X}}$ .

<sup>3</sup> In the RKHS norm.

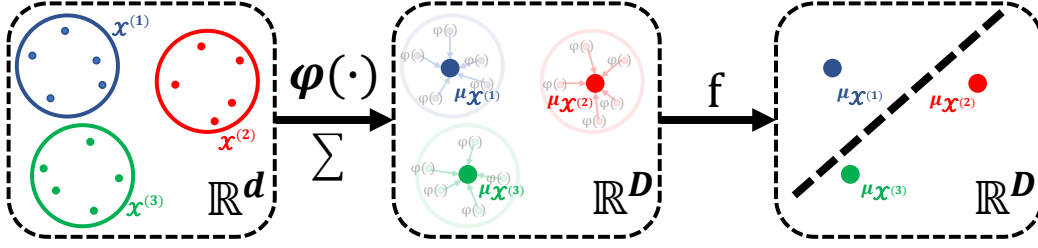


Fig. 2: The pipeline of CKME to process the dataset and train the classifier. The left rectangle shows a dataset with 3 sample-sets and each sample-set contains 5 features vectors in the original feature space  $\mathbb{R}^d$ . In the middle rectangle, we use  $\varphi(\cdot)$  to transform the data into random Fourier feature space  $\mathbb{R}^D$  and compute the mean embedding  $\mu_{\mathcal{X}^{(1)}}$ ,  $\mu_{\mathcal{X}^{(2)}}$ ,  $\mu_{\mathcal{X}^{(3)}}$  for every sample-set (eq. 4). Finally, in the right rectangle, we train a linear discriminative model  $f$  (eq. 6) upon the mean embeddings to predict the label of each sample-set.

**Linear Classifier with Interpretable Scores** With the mean embedding of sample-sets  $\{\mu_{\mathcal{X}^{(k)}}\}_{k=1}^N$ ,  $\mu_{\mathcal{X}^{(k)}} \in \mathbb{R}^D$ , we can build a discriminative model  $f : \mathbb{R}^D \rightarrow \mathbb{R}$  to predict their labels. If we choose  $f$  as a linear model (e.g. linear SVM or logistic regression), then  $f(\mu_{\mathcal{X}})$  can be generally expressed as

$$f(\mu_{\mathcal{X}^{(k)}}) = \mu_{\mathcal{X}^{(k)}}^T \beta + b = \frac{1}{n_k} \sum_{i=1}^{n_k} \underbrace{\varphi(x^{(k,i)})^T \beta + b}_{s^{(k,i)}} = \frac{1}{n_k} \sum_{i=1}^{n_k} s^{(k,i)}, \quad (6)$$

where  $\beta \in \mathbb{R}^D$  and  $b \in \mathbb{R}$  are the weight and the bias of the linear model. We summarize the pipeline of CKME to process the dataset and train the classifier in Fig. 2.

From eq. 6, we can express the output response of  $f$  as the mean of all  $s^{(k,i)}$ . We denote  $s^{(k,i)}$  the score of the  $i$ -th cell in the sample-set  $\mathcal{X}^{(k)}$ . This formulation naturally allows to quantify and interpret the contribution of every sub-selected cell to the final prediction, which can potentially lead to an improved understanding of biological phenomena and enable better diagnoses and treatment for patients.

**Kernel Herding** When using random features (eq. 4),  $\mu_{\mathcal{X}}$  may be understood as the average of random features for cells found in a sample-set. Predicted outputs based on  $\mu_{\mathcal{X}}$  (eq. 6) may be further interpreted as the average “score” of cells in the respective sample-set. However, sample-sets may contain many (hundreds of) thousands of cells, making it cumbersome to analyze and synthesize the cell scores in a sample-set. To ease interpretability, we propose to subselect cells in the sample-set in a way that yields a similar embedding to the original sample-set. That is, we wish to find a subset  $\hat{\mathcal{X}} \subset \mathcal{X}$  such that  $\mu_{\hat{\mathcal{X}}} \approx \mu_{\mathcal{X}}$ , which implies that one may make similar inferences using a smaller (easier to interpret) subset of cells as with the original sample-set. Although a uniformly random subsample of  $\mathcal{X}$  would provide a decent approximation  $\mu_{\hat{\mathcal{X}}}$  for large enough cardinality ( $|\hat{\mathcal{X}}|$ ), it is actually a suboptimal way of constructing an approximating subset. Instead, we propose to better construct synthesized subsets (especially for small cardinalities) using kernel herding (KH) [8]. KH can provide a subset of  $m$  points that approximates the mean embedding as well as  $m^2$  uniformly sub-sampled points. We expound on KH for producing subsets of key predictive cells in Algorithm 1. We denote the dataset with the sub-selected sets as  $\hat{\mathcal{D}} = \{(\hat{\mathcal{X}}^{(k)}, y^{(k)})\}_{k=1}^N$ .

**Clustering Analysis with CKME Scores** Traditionally, practitioners have employed unsupervised clustering to partition cells and create associated immunological features by computing the proportion of

---

**Algorithm 1** COMPUTE THE SUB-SELECTED SAMPLE SET AND ITS MEAN EMBEDDING
 

---

**Require:** A sample-set  $\mathcal{X}$ , number of cells kept after sub-selection  $m$ , dimensionality of the random feature space  $D$ , kernel hyperparameter  $\gamma$ .

```

1: # Compute Random Fourier Frequency Features
2: Compute  $\mathbf{W} \in \mathbb{R}^{d \times \frac{D}{2}}$  by sampling its elements independently  $\mathbf{w}_{i,j} \sim \mathcal{N}(0, \frac{1}{\gamma})$ 
3: for each  $x^{(i)} \in \mathcal{X}$  do
4:    $x_{\text{rand}}^{(i)} \leftarrow [\sin(\mathbf{W}^T x^{(i)}), \cos(\mathbf{W}^T x^{(i)})] \in \mathbb{R}^D$ , where  $[\cdot, \cdot]$  denotes concatenation.
5: end for
6: # Sub-selection with Kernel Herding
7: Initialize  $j \leftarrow 1$ ,  $\hat{\mathcal{X}}_{\text{rand}} \leftarrow \emptyset$ ,  $\hat{\mathcal{X}} \leftarrow \emptyset$ ,  $\theta_0 \leftarrow \frac{1}{n} \sum_{i=1}^n x_{\text{rand}}^{(i)}$ ,  $\theta_t \leftarrow \theta_0$ 
8: while  $j \leq m$  do
9:    $i^* \leftarrow \arg \max_i \theta_t^T x_{\text{rand}}^{(i)}$ 
10:   $\hat{\mathcal{X}}_{\text{rand}} \leftarrow \hat{\mathcal{X}}_{\text{rand}} \cup \{x_{\text{rand}}^{(i^*)}\}$ ,  $\hat{\mathcal{X}} \leftarrow \hat{\mathcal{X}} \cup \{x^{(i^*)}\}$ 
11:   $\theta_t \leftarrow \theta_t + \theta_0 - x_{\text{rand}}^{(i^*)}$ 
12:   $j \leftarrow j + 1$ 
13: end while
14: # Compute the mean embedding of the Sub-selected Sample-set
15:  $\mu_{\hat{\mathcal{X}}} = \frac{1}{m} \sum_{z \in \hat{\mathcal{X}}_{\text{rand}}} z$ 
16: return  $\hat{\mathcal{X}}$ ,  $\mu_{\hat{\mathcal{X}}}$ 

```

---

cells in each sample-set assigned to each cluster [5,21,25]. Specifically, one can first use k-means to cluster the feature vectors  $x \in \bigcup_{k=1}^N \mathcal{X}^{(k)}$  of all the cells in the multi-sample dataset. Since the union of all sample-sets,  $\bigcup_{k=1}^N \mathcal{X}^{(k)}$ , often results in a very large set of instances, the cluster analysis is typically done using down-sampled sets  $\bigcup_{k=1}^N \tilde{\mathcal{X}}^{(k)}$ , where  $\tilde{\mathcal{X}}^{(k)}$  is commonly selected as a uniform subsample of  $\mathcal{X}^{(k)}$ . Once the cluster analysis is optimized, one obtains  $C$  cluster centers,  $\nu_1, \dots, \nu_C$ . For each sample-set  $\mathcal{X}^{(k)}$ , one can compute the ratio of cells assigned to each cluster; i.e. compute  $r_1^{(k)}, r_2^{(k)}, \dots, r_C^{(k)}$  where  $r_j^{(k)} = \frac{1}{|\mathcal{X}^{(k)}|} \sum_{x \in \mathcal{X}^{(k)}} \mathbb{I}\{j = \arg \min_l \|\nu_l - x\|\}$ . These ratios can be used as a feature vector  $\vec{r}^{(k)} = [r_1^{(k)}, r_2^{(k)}, \dots, r_C^{(k)}]$  for classification models. I.e. one may fit a linear model  $\vec{r}^{(k)T} \beta + b$  with learned coefficients  $\beta$  (and bias  $b$ ). We denote this traditional method as *Cluster Classify* and will evaluate it as a baseline in the experiments.

We propose to combine cell scores computed by CKME (eq. 6) with a cluster analysis to further interpret CKME predictions. Recall that CKME can compute a score  $s^{(k,i)}$  for every feature vector  $\hat{x}^{(k,i)}$  in the KH sub-selected sample-set  $\hat{\mathcal{X}}^{(k)}$ . With these cell scores, we can also assign a score to every cluster as  $s_c = \frac{1}{|G_c|} \sum_{\hat{x}^{(k,i)} \in G_c} s^{(k,i)}$ , where  $s_c$  denotes the score assigned to the  $c$ -th cluster and  $G_c$  denotes the set of features in  $\hat{\mathcal{D}}$  assigned to the  $c$ -th cluster,  $G_c = \{x \in \bigcup_{k=1}^N \hat{\mathcal{X}}^{(k)} \mid c = \arg \min_l \|\nu_l - x\|\}$ . Alternatively, we may assign scores to clusters by directly using the learned random-feature linear model in eq. 6 to transform the centroids as  $s_c = \varphi(\nu_c)^T \beta + b$ . Interestingly, we find that both cluster scoring approaches lead to approximately the same cluster scores and identical downstream predictions<sup>4</sup>. This observation attests to the robustness of cell scores computed by CKME and kernel herding sub-selection since the model was never explicitly trained with respect to these cluster analyses. With a score assigned to every cluster, we can predict the label of  $\hat{\mathcal{X}}^{(k)}$  using a convex combination of the cluster scores according to the cluster frequencies found in  $\hat{\mathcal{X}}^{(k)}$ . I.e. predict using  $\hat{f}(\hat{\mathcal{X}}^{(k)}) = \sum_{c=1}^C \hat{r}_c^{(k)} s_c$ , where  $\hat{r}_c^{(k)}$  is the proportion of cells in  $\hat{\mathcal{X}}^{(k)}$  assigned to cluster  $c$ . This intuitive predictor uses the score of each cluster weighted by the presence of that cluster in  $\hat{\mathcal{X}}^{(k)}$ . We denote this approach as *Cluster Comb CKME* and compare it to CKME as a baseline in the

---

<sup>4</sup> We report results using the first averaging method for producing cluster scores.

experiments. Note that although *Cluster Comb CKME* is a linear model,  $\sum_{c=1}^C \hat{r}_c^{(k)} s_c$ , it is one that is fit *indirectly* through our learned cell scores  $s_c$ . To validate and compare our cell scores, we also use other methods such as MELD [6] to compute a score for every cell and derive a score to every cluster for prediction as above. The predictions using the MELD cluster scores (derived from MELD cell scores) are denoted as *Cluster Comb MELD*.

**Flow and Mass Cytometry Datasets Used in Experiments** In all experiments, we used publicly available, multi-sample-set flow and mass cytometry (CyTOF) datasets. Each sample-set consists of several protein markers measured across individual cells. Here, we briefly introduce the multi-sample and publicly available flow and mass cytometry datasets used in all experiments.

*Preeclampsia* The preeclampsia CyTOF dataset profiles 11 women with preeclampsia and 12 healthy women throughout their pregnancies. Sample-sets corresponding to profiled samples from women are publicly available and were downloaded from Flow Repository (<http://flowrepository.org/id/FR-FCM-ZYRQ>). Our experiments focused on uncovering differences between healthy and preeclamptic women.

*HVTN* The HVTN (HIV Vaccine Trials Network) is a Flow Cytometry dataset that profiled T-cells across 96 samples that were each subjected to stimulation with either Gag or Env proteins<sup>5</sup> [1]. The data are publicly available and were downloaded from Flow Repository under Repository ID FR-FCM-ZZZV (<http://flowrepository.org/id/FR-FCM-ZZZV>). Our experiments focused on uncovering differences from Gag and Env stimulated samples.

*COVID-19* The COVID-19 dataset analyzes cytokine production by PBMCs derived from COVID-19 patients. The dataset profiles healthy patients, as well patients with moderate and severe covid cases. Specifically, the dataset consists of samples from 49 total individuals and is comprised of 6 healthy, 23 labeled intensive-care-unit (ICU) with moderately severe COVID, and 20 Ward (non-ICU, but covid-severe) labeled individuals with severe COVID cases, respectively. The data are publicly available and were downloaded from Flow Repository under Repository ID FR-FCM-Z2KP (<http://flowrepository.org/id/FR-FCM-Z2KP>). Our experiments focused on uncovering differences between sample-sets from ICU and Ward patients.

### 3 Results

Given the limited number of sample-sets, we used 5-fold cross-validation to report the classification accuracies on the three datasets. We tuned the hyperparameter (i.e. the bandwidth parameter  $\gamma$  and the dimensionality  $D$  of the random Fourier frequency features space) on the validation set. On the HVTN and the Preeclampsia datasets,  $\gamma$  was set to 1 while on the COVID-19 dataset  $\gamma$  was set to 6. The dimensionality  $D$  was set to 2000 for all datasets. We report classification the accuracies of three classifiers, including, logistic regression, Linear SVM, and SVM with RBF kernel.

#### 3.1 Baselines

We focused on comparing CKME a current state-of-the-art method CytoSet [27]. CytoSet employs a deep learning model similar to Deep Set [28] to handle set data. CytoSet employs a permutation invariant architecture that uses intermediate permutation *equivariant* neural network layers. As a result, the sample-set featurization that CytoSet achieves, while discriminative and accurate, is opaque and a black box, making it difficult

<sup>5</sup> Note these are proteins meant to illicit functional responses in immune cell-types.

Table 1: Classification accuracy on predicting stimulation with Gag or Env in the HVTN dataset. Standard deviations are computed from 5 independent runs.

| Methods                                | Accuracy(%)                        | # Parameters(k) |
|--|------------------------------------|-----------------|
| CytoSet                                | <b>90.52 <math>\pm</math> 2.26</b> | 300.2           |
| <i>Cluster Comb MELD</i>               | 64.52 $\pm$ 0.92                   | <b>0.01</b>     |
| <i>Cluster Comb CKME</i>               | <b>90.68 <math>\pm</math> 1.69</b> | <b>0.01</b>     |
| <i>Cluster Classify</i>                | 78.66 $\pm$ 2.86                   | 0.02            |
| Naive Mean Featurization               | 64.24 $\pm$ 3.17                   | <b>0.01</b>     |
| CKME (Linear SVM) w/ Unif. Subsampling | 80.26 $\pm$ 1.53                   | 2.0             |
| CKME (RBF SVM)                         | 72.95 $\pm$ 3.09                   | 2.0             |
| CKME (LR)                              | 84.42 $\pm$ 3.30                   | 2.0             |
| CKME (Linear SVM)                      | <b>90.68 <math>\pm</math> 1.69</b> | 2.0             |

to analyze downstream for biological discoveries. In addition, CytoSet usually contains millions of parameters, further obfuscating the underlying predictive mechanisms. As shown in [27], other deep learning methods such as CellCNN [2] and CytoDx [15] can be regarded as a special case of CytoSet, but are not as expressive as CytoSet. CytoSet was run using its public implementation (<https://github.com/CompCy-lab/cytoSet>). We also compared to the two baselines, including, *Cluster Comb* and *Cluster Classify*, introduced in the section “Clustering Analysis with CKME Scores”.

### 3.2 Classification Accuracy

**HVTN dataset** We report the experimental results on the HVTN dataset in Table 1. We observed that CKME with Linear SVM classifier outperforms all the baselines. Compared to CytoSet, CKME contains significantly fewer parameters while achieving slightly higher accuracy. Fig. 3 shows the classification accuracies of CKME with different numbers of cells selected by KH. We found that the accuracy quickly saturates with as few as 50 cells sub-selected for every sample-set, confirming the strong capacity of KH to maintain the distribution of the original sample-sets after sub-selection.

We performed two ablation studies. For the first study, we trained CKME without using random Fourier features (Naive Mean Featurization). In this case, we still used KH to sub-select  $m$  cells but represented the summarized sample-set in the original feature space as  $\bar{\mathbf{x}}^{(k)} = \frac{1}{m} \sum_{j=1}^m \hat{\mathbf{x}}^{(k,j)} \in \mathbb{R}^d$ . In the second study, we sub-selected  $m$  cells under uniform selection, instead of Kernel Herding (CKME w/ Unif. Subsampling). Both of these two baselines resulted in poor classification accuracy. This shows that simple summary statistics ( $\bar{\mathbf{x}}^{(k)}$ , the mean of input features) does not suffice for classification; in contrast, the random feature kernel mean embedding is able to provide an expressive enough summary of sample-sets. Furthermore, the drop in performance from KH with uniform subsampling confirms that KH is a superior method for synthesizing sample-sets with key cells.

We also report the performance of clustering analysis (k-means with 10 clusters). Interestingly, we find that *Cluster Comb* using the scores computed by CKME (Linear SVM) achieves identically strong performance to CKME (Linear SVM). To investigate this phenomenon, we separately show the histogram of

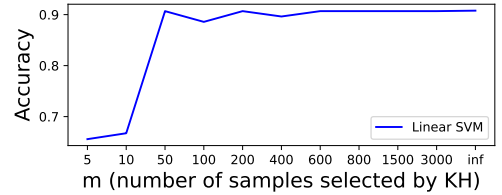


Fig. 3: The influence of the number of cells selected by KH,  $m$ , on the classification accuracy.  $m = \text{“inf”}$  means no sub-selection.



clustering assignments for both the negative (Gag stimulated) and the positive (Env stimulated) class (Appendix Fig. 1). We also show the score of each cluster computed by CKME. We can see that there are more cells in the negative class assigned to clusters with negative scores (e.g. Cluster 1 and 3) compared to cells in the positive class. Perhaps even more interesting, we observed that the linear model on cluster frequency features *indirectly trained* through CKME’s cell scores (*Cluster Comb CKME*) generalizes better than a linear model that was *directly trained* on the cluster frequency features (*Cluster Classify*). This suggests that cell scores that we learn provide a helpful inductive bias when aggregated that is lost when only summarizing sample-sets using cluster frequencies. Moreover, discriminative capabilities and strong signals given by aggregating the individual cell scores within a cluster allow for the rapid identification of cell-populations that are most prominently driving a particular clinical outcome. Alternatively, when using the scores computed by MELD, *Cluster Comb MELD* an lower accuracy of 64.52 % was achieved, indicating the MELD scores are not discriminative enough. MELD scores most likely lack discriminative capability in our experiment because MELD computes scores that prioritize the identification of cells associated with an experimental condition or clinical label, rather than scores that measure the contribution of every single cell to the predicted sample-set label.

The results of CytoSet were computed with  $m = 256$  cells sub-selected for every sample-set and the CytoSet model contains 3 blocks, which is shown in [27] to achieve the best performance on this dataset. The results of CKME in Table 1 are computed with  $m = 200$  cells sub-selected.

**Preeclampsia dataset** We report the experimental results on the Preeclampsia dataset in Table 2. On this dataset, CKME (Linear SVM) outperforms all the other baselines, including CytoSet. The relative performance of different methods on this dataset follows a similar trend that is observed in the HVTN dataset. We trained CytoSet with  $m = 256$  cells sub-selected and the CytoSet model containing 1 block. This configuration was chosen using a validation set. When using more blocks, we found CytoSet suffered from overfitting. The results of CKME shown in Table 2 were computed with  $m = 200$ .

**COVID-19 dataset** We report the results on the COVID-19 dataset in Table 3. We observed that CytoSet and CKME with logistic regression classifier CKME (LR) achieves similar performance and outperform other methods on this dataset. However, CKME (LR) has fewer parameters compared to CytoSet. The relative performance of other methods is similar to that of the previous two datasets. We trained CytoSet with  $m = 256$  sub-selected cells and 3 blocks. This configuration was chosen using a validation set. The results of CKME in Table 3 were computed with  $m = 50$ , which is selected on the validation set.

### 3.3 Biological Validation

On the Preeclampsia dataset, we used our scores to prioritize cells that were different between control (healthy) and preeclamptic women. Cells across sample-sets were clustered into one of 10 clusters. We then computed the mean score of the cells assigned to each cluster. In doing so, we prioritized cluster 2, based on its highly negative score, implying that it likely contained a large number of cells predicted as “control” (see Appendix Fig. 2). The prominent protein markers expressed in cluster 2 were CD3, CD4, CD45RA, and MAPKAPK2 and indicated this is a cell-population of naive  $CD4^+$  T cells expressing MAPKAPK2 (Fig. 4a). Previous work showed that women with preeclampsia exhibit a decrease in MAPKAPK2<sup>+</sup> naive  $CD4^+$  T-cells during the course of pregnancy, while healthy, women exhibit an increase [14].

We first compared the distributions of frequencies of cells assigned to cluster 2 (e.g. this population of naive  $CD4^+$  T cells expressing MAPKAPK2) between sample-sets from preeclamptic and healthy control women (Fig. 4b). Consistent with our previous observations, sample-sets from control women had a statistically

Table 2: Classification results on the Preeclampsia dataset to predict healthy from preeclamptic women. Standard deviations are computed from 5 independent runs.

| Methods                                | Accuracy(%)                        | # Parameters(k) |
|--|------------------------------------|-----------------|
| CytoSet                                | $58.45 \pm 3.37$                   | 80.0            |
| <i>Cluster Comb MELD</i>               | $59.64 \pm 3.47$                   | <b>0.01</b>     |
| <i>Cluster Comb CKME</i>               | <b><math>62.60 \pm 2.39</math></b> | <b>0.01</b>     |
| <i>Cluster Classify</i>                | $56.64 \pm 4.16$                   | 0.02            |
| Naive Mean Featurization               | $57.60 \pm 4.20$                   | 0.03            |
| CKME (Linear SVM) w/ Unif. Subsampling | $55.52 \pm 4.33$                   | 2.0             |
| CKME (RBF SVM)                         | $55.91 \pm 3.29$                   | 2.0             |
| CKME (LR)                              | $58.56 \pm 3.72$                   | 2.0             |
| CKME (Linear SVM)                      | <b><math>62.60 \pm 2.39</math></b> | 2.0             |

Table 3: Classification results on the COVID-19 dataset to predict Healthy from Ward Patients. Standard deviations are computed from 5 independent runs.

| Methods                        | Accuracy(%)                        | # Parameters(k) |
|--------------------------------|------------------------------------|-----------------|
| CytoSet                        | <b><math>86.67 \pm 1.73</math></b> | 330.0           |
| <i>Cluster Comb MELD</i>       | $59.16 \pm 3.72$                   | <b>0.01</b>     |
| <i>Cluster Comb CKME</i>       | <b><math>86.38 \pm 1.92</math></b> | <b>0.01</b>     |
| <i>Cluster Classify</i>        | $76.92 \pm 2.05$                   | 0.02            |
| Naive Mean Featurization       | $83.07 \pm 2.29$                   | 0.03            |
| CKME (LR) w/ Unif. Subsampling | $84.28 \pm 1.74$                   | 2.0             |
| CKME (Linear SVM)              | $77.72 \pm 2.83$                   | 2.0             |
| CKME (RBF SVM)                 | $79.77 \pm 2.49$                   | 2.0             |
| CKME (LR)                      | <b><math>86.38 \pm 1.92</math></b> | 2.0             |

significantly higher proportion of cells assigned to cluster 2 in comparison to preeclamptic women (see Fig. 4b with a p-value of  $p = 0.038$  under a Wilcoxon Rank Sum Test). As a complementary visualization, we constructed a  $k$ -nearest neighbor graph between sample-sets according to the computed frequencies across all cell-types (Fig. 4c-d). Here, each node represents a sample-set and an edge represents sufficient similarity between a pair of sample-sets according to the frequencies of cells across cell-populations. In Fig. 4c, sample-sets (nodes) are colored by the probability of their cells belonging to cluster 2. In comparison to sample-sets (nodes) colored by their ground-truth labels (Fig. 4d), we observed that control, healthy sample-sets such as the densely connected set of blue nodes in the bottom of Fig. 4d tend to have high frequencies of cells assigned to cluster 2.

## 4 Discussion and Conclusion

Here, we introduced CKME (Cell Kernel Mean Embedding) as a method to link cellular heterogeneity in the immune system to clinical or external variables of interest, while simultaneously facilitating biological interpretability. As high-throughput single-cell immune profiling techniques are being readily applied in clinical settings [12,14,11], and there are critical needs to 1) accurately diagnose or predict a patient’s future clinical outcome and to 2) explain the particular cell-types driving these predictions. While several recent

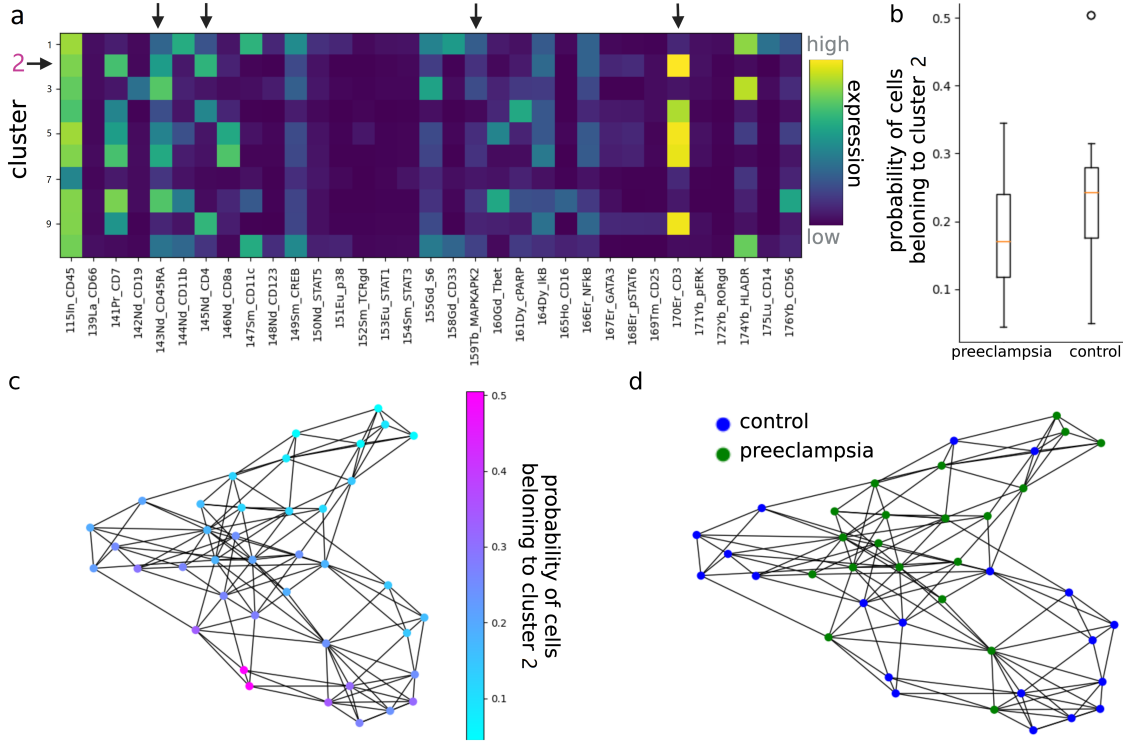


Fig. 4: Our predicted scores prioritized cluster 2 (CD4<sup>+</sup> naive T-cells) as cell-population likely to have frequency differences between control and preeclamptic samples. **a** Cluster 2 was identified to correspond to a population of MAPKAPK2<sup>+</sup> CD4<sup>+</sup> naive T-cells according to protein markers (denoted with arrows). **b** The distributions of frequencies of cells assigned to cluster 2 in sample-sets from preeclamptic and control women. **c** A  $k$ -NN graph connecting samples-sets (nodes) according to computed frequencies across cell-populations reveals a higher frequency of cells assigned to cluster 2 in control samples-sets. **d** The  $k$ -NN graph from (c), with each sample-set (node) colored by its ground-truth label.

bioinformatics approaches have successfully been able to specify [5,25,15] or learn [2,27] immunological features that can accurately predict a patient's clinical outcome. These existing methods, however, have struggled to readily communicate the prominent immune cell-types driving the differences between distinct clinical phenotypes without extensive manual analysis and interpretation. Independent of clinical outcome classification, MELD [7] was recently introduced to score cells based on their association with a particular clinical or experimental condition, but the per-cell scores are not intended to be discriminative in nature. In contrast, CKME simultaneously achieves state-of-the-art classification accuracy and computes per-cell responses that are discriminative of patient phenotype when aggregated.

In summary, CKME enables more comprehensive, automated analysis and interpretation of multi-patient flow and mass cytometry datasets and will accelerate the understanding of how immunological dysregulation affects particular clinical phenotypes.

## References

1. Aghaeepour, N., Finak, G., Hoos, H., Mosmann, T.R., Brinkman, R., Gottardo, R., Scheuermann, R.H.: Critical assessment of automated flow cytometry data analysis techniques. *Nature methods* **10**(3), 228–238 (2013)
2. Arvaniti, E., Claassen, M.: Sensitive detection of rare disease-associated cell subsets via representation learning. *Nature communications* **8**(1), 1–10 (2017)
3. Bendall, S.C., Simonds, E.F., Qiu, P., El-ad, D.A., Krutzik, P.O., Finck, R., Bruggner, R.V., Melamed, R., Trejo, A., Ornatsky, O.I., et al.: Single-cell mass cytometry of differential immune and drug responses across a human hematopoietic continuum. *Science* **332**(6030), 687–696 (2011)
4. Berlinet, A., Thomas-Agnan, C.: Reproducing kernel Hilbert spaces in probability and statistics. Springer Science & Business Media (2011)
5. Bruggner, R.V., Bodenmiller, B., Dill, D.L., Tibshirani, R.J., Nolan, G.P.: Automated identification of stratifying signatures in cellular subpopulations. *Proceedings of the National Academy of Sciences* **111**(26), E2770–E2777 (2014)
6. Burkhardt, D.B., Stanley, J.S., Tong, A., Perdigo, A.L., Gigante, S.A., Herold, K.C., Wolf, G., Giraldez, A.J., van Dijk, D., Krishnaswamy, S.: Quantifying the effect of experimental perturbations at single-cell resolution. *Nature biotechnology* **39**(5), 619–629 (2021)
7. Burkhardt, D.B., Stanley, J.S., Tong, A., Perdigo, A.L., Gigante, S.A., Herold, K.C., Wolf, G., Giraldez, A.J., van Dijk, D., Krishnaswamy, S.: Quantifying the effect of experimental perturbations at single-cell resolution. *Nature Biotechnology* pp. 1–11 (2021)
8. Chen, Y., Welling, M., Smola, A.: Super-samples from kernel herding. In: *Proceedings of the Twenty-Sixth Conference on Uncertainty in Artificial Intelligence*. pp. 109–116 (2010)
9. Cortes, C., Vapnik, V.: Support-vector networks. *Machine learning* **20**(3), 273–297 (1995)
10. Davis, M.M., Tato, C.M., Furman, D.: Systems immunology: just getting started. *Nature immunology* **18**(7), 725 (2017)
11. Fallahzadeh, R., Verdonk, F., et al.: Objective activity parameters track patient-specific physical recovery trajectories after surgery and link with individual preoperative immune states. *Annals of Surgery* (2021)
12. Ganio, E.A., Stanley, N., Lindberg-Larsen, V., et al.: Preferential inhibition of adaptive immune system dynamics by glucocorticoids in patients after acute surgical trauma. *Nature communications* **11**(1), 1–12 (2020)
13. Gretton, A., Borgwardt, K.M., Rasch, M.J., Schölkopf, B., Smola, A.: A kernel method for the two-sample problem. *Journal of Machine Learning Research* **1**, 1–10 (2008)
14. Han, X., Ghaemi, M.S., et al.: Differential dynamics of the maternal immune system in healthy pregnancy and preeclampsia. *Frontiers in immunology* **10**, 1305 (2019)
15. Hu, Z., Glicksberg, B.S., Butte, A.J.: Robust prediction of clinical outcomes using cytometry data. *Bioinformatics* **35**(7), 1197–1203 (2019)
16. Liechti, T., Weber, L.M., Ashhurst, T.M., Stanley, N., Prlic, M., Van Gassen, S., Mair, F.: An updated guide for the perplexed: cytometry in the high-dimensional era. *Nature Immunology* **22**(10), 1190–1197 (2021)
17. Mika, S., Schölkopf, B., Smola, A.J., Müller, K.R., Scholz, M., Rätsch, G.: Kernel pca and de-noising in feature spaces. In: *NIPS*. vol. 11, pp. 536–542 (1998)
18. Molnar, C.: *Interpretable machine learning*. Lulu. com (2020)
19. Muandet, K., Fukumizu, K., Sriperumbudur, B., Schölkopf, B.: Kernel mean embedding of distributions: A review and beyond. *Foundations and Trends in Machine Learning* **10**(1-2), 1–141 (2017)
20. Qi, C.R., Su, H., Mo, K., Guibas, L.J.: Pointnet: Deep learning on point sets for 3d classification and segmentation. In: *Proceedings of the IEEE conference on computer vision and pattern recognition*. pp. 652–660 (2017)
21. Qiu, P., Simonds, E.F., Bendall, S.C., Gibbs, K.D., Bruggner, R.V., Linderman, M.D., Sachs, K., Nolan, G.P., Plevritis, S.K.: Extracting a cellular hierarchy from high-dimensional cytometry data with spade. *Nature biotechnology* **29**(10), 886–891 (2011)
22. Rahimi, A., Recht, B., et al.: Random features for large-scale kernel machines. In: *NIPS*. vol. 3, p. 5. Citeseer (2007)
23. Schölkopf, B., Herbrich, R., Smola, A.J.: A generalized representer theorem. In: *International conference on computational learning theory*. pp. 416–426. Springer (2001)

24. Shi, Y., Oliva, J., Niethammer, M.: Deep message passing on sets. In: Proceedings of the AAAI Conference on Artificial Intelligence. vol. 34, pp. 5750–5757 (2020)
25. Stanley, N., Stelzer, I.A., et al.: Vopo leverages cellular heterogeneity for predictive modeling of single-cell data. *Nature communications* **11**(1), 1–9 (2020)
26. Vovk, V.: Kernel ridge regression. In: Empirical inference, pp. 105–116. Springer (2013)
27. Yi, H., Stanley, N.: Cytoset: Predicting clinical outcomes via set-modeling of cytometry data. In: Proceedings of the 12th ACM Conference on Bioinformatics, Computational Biology, and Health Informatics. BCB '21, Association for Computing Machinery (2021)
28. Zaheer, M., Kottur, S., Ravanbakhsh, S., Poczos, B., Salakhutdinov, R.R., Smola, A.J.: Deep sets. *Advances in Neural Information Processing Systems* **30** (2017)

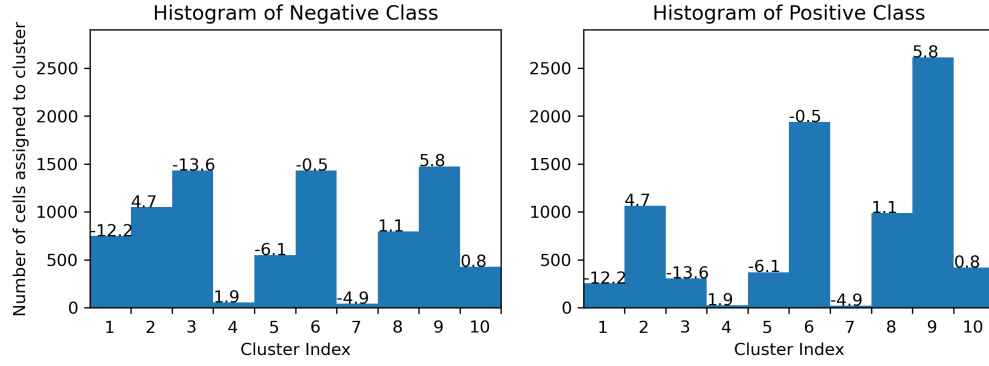


Fig. 1: The histogram of the clustering assignments on the HVTN dataset. The score of each cluster is shown on the top of each corresponding bar.

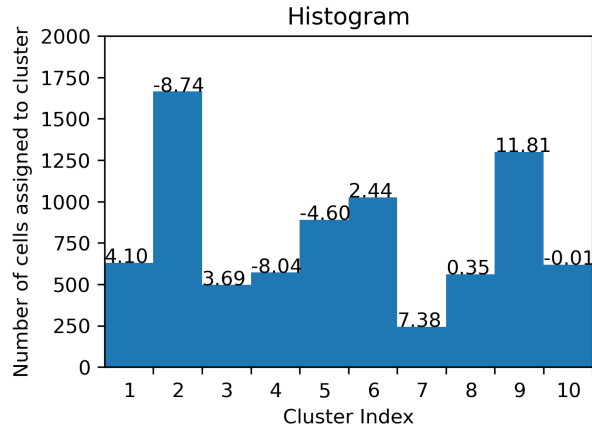


Fig. 2: We computed the frequency of (e.g. number of) cells assigned to each of 10 clusters, or cell-populations. We further computed the mean of our computed scores for the cells assigned to each cluster. We prioritized cluster 2, due to its extreme negative score of -8.74, indicating an abundance of cells from healthy, control sample-sets.